e-ISSN: 2582-5208
International Research Journal of Modernization in Engineering Technology and Science
(Peer-Reviewed, Open Access, Fully Refereed International Journal)
Volume:07/Issue:01/January-2025 Impact Factor- 8.187 www.irjmets.com

NUMERICAL INVESTIGATION OF HEAT TRANSFER IN RECTANGULAR MICROCHANNELS AND THERMAL SINKS USING OPTIMIZED PIN CONFIGURATIONS

Masoud Hatami Garousi*1, Peyman Norouzi Givi*2, Latifeh Arazipoor*3, Narges Fathali*4

*1Department Of Engineering For Industrial Systems And Technologies, University Of Parma, 43124 Parma, Italy.

*2Faculty Of Mechanical Engineering, Istanbul Technical University, Istanbul, Turkey.

*3Department Of Civil Engineering, Chemistry And Environmental, University Of Genova, Genova, Italy.

*4Department Of Food And Drug, University Of Parma, Parma, Italy.

DOI : https://www.doi.org/10.56726/IRJMETS65903

ABSTRACT

This study investigates the thermal performance of rectangular microchannels using computational fluid dynamics (CFD) simulations, validated against experimental data. Various geometric configurations, including pins positioned at the entrance, exit, and distributed along the entire channel, were analyzed to optimize heat transfer. The results reveal that the "Pin in Front" configuration provides the best balance, outperforming the "All pin" configuration by 6% and the "Pin in back" configuration by 12% in thermal performance at low Reynolds numbers. At higher Reynolds numbers, the differences reduce to 2% and 5%, respectively, while the "Pin in Front" configuration consistently exhibits superior performance. Furthermore, increasing the pin height from 400 μm to 700 μm improves the Nusselt number by 22.5% at low Reynolds numbers and 20.5% at high Reynolds numbers, highlighting the importance of surface modifications in enhancing convective heat transfer. These findings provide critical insights for the design and optimization of advanced microchannel heat sinks for high-power applications.

Keywords: Microchannels, Heat Transfer, CFD Simulation, Thermal Optimization, Geometric Modifications.

I. INTRODUCTION

Microchannels have emerged as critical components in advanced thermal management systems due to their exceptional ability to dissipate high heat fluxes in compact spaces. Their high surface area-to-volume ratio allows for efficient heat transfer, making them indispensable in electronics cooling, biomedical devices, and micro-scale heat exchangers[1,2]. However, microchannels are not without challenges, including high-pressure drops, potential flow maldistribution, and thermal hotspots[3]. Addressing these limitations is vital for optimizing microchannel designs and improving their performance.

The concept of microchannel heat sinks was first introduced by Tuckerman and Pease [4], who demonstrated that reducing hydraulic diameters significantly enhances thermal performance. Since then, extensive research has explored various geometric and operational modifications. For example, Sahar et al. [5]investigated the impact of hydraulic diameter and aspect ratio, finding that larger hydraulic diameters increase Nusselt numbers but may lead to higher pressure drops. Similarly, studies by Baraty Beni et al. [6] demonstrated that sinusoidal microchannel geometries improve thermal performance, albeit at the cost of increased pressure drops. Several studies have focused on surface modifications to enhance turbulence and heat transfer. Rimbault et al. [7] showed that nanofluids, such as CuO-water mixtures, can improve heat transfer coefficients while influencing friction factors and laminar-to-turbulent transition points. Similarly, Qu and Mudawar [8] highlighted the role of three-dimensional conjugate heat transfer models in accurately predicting fluid and thermal behavior in microchannels.

Computational fluid dynamics (CFD) has become a cornerstone in microchannel research, enabling detailed simulations of fluid flow and thermal interactions. Nekoubin [9] employed single-domain formulations to analyze the effects of electrical double layers on microchannel heat transfer, providing insights into thermally

e-ISSN: 2582-5208
International Research Journal of Modernization in Engineering Technology and Science
(Peer-Reviewed, Open Access, Fully Refereed International Journal)
Volume:07/Issue:01/January-2025 Impact Factor- 8.187 www.irjmets.com

developing regions. Wang et al. [10] explored forced convection cooling using CFD, identifying optimal Reynolds numbers and channel geometries for effective heat removal.

To further enhance microchannel efficiency, ribbed and pin-finned designs have been extensively studied. Ghani et al. [11] demonstrated that these configurations disrupt boundary layers and promote fluid mixing, thereby improving heat transfer rates. Meanwhile, experimental studies by Xia et al. [3] revealed that the transition from laminar to turbulent flow in ribbed microchannels occurs at lower Reynolds numbers compared to smooth channels, facilitating earlier thermal performance gains. Nanofluids have also garnered significant attention for their ability to enhance microchannel performance. Singh et al. [12] observed that alumina-water nanofluids improve heat transfer rates while reducing entropy generation, particularly under turbulent flow conditions. However, challenges such as particle agglomeration and increased pumping power requirements must be addressed for practical applications.

Advanced manufacturing techniques have further expanded the design possibilities for microchannels. For instance, microfabrication and additive manufacturing methods enable the creation of intricate channel geometries and integrated heat sinks. Wei et al. [13] demonstrated that microchannel arrays with tailored cross-sections achieve higher heat flux dissipation compared to conventional designs, making them suitable for high-power applications such as laser diode cooling. Despite these advancements, the field continues to grapple with questions related to the scaling of experimental findings to real-world applications. For example, studies by Kuppusamy et al [14] and Li, Jie. [15] highlighted discrepancies between theoretical predictions and experimental results, particularly in the context of nanofluid behavior in microchannels. Fallahzadeh et al. [16–18] conducted a CFD-based investigation into single-loop triple-diameter pulsating heat pipes, revealing that optimized inner diameters significantly reduce thermal resistance and enhance full circulation flow patterns. Similarly, their findings demonstrated that triple-diameter configurations outperform single- and dual-diameter designs in thermal performance under low heat inputs. This work contributes to the understanding of geometry-driven thermal management solutions. These findings underscore the need for comprehensive validation frameworks that integrate numerical, experimental, and analytical approaches.

This study aims to contribute to this evolving field by leveraging CFD simulations to validate microchannel performance against experimental data. The research then explores geometric enhancements, including various pin configurations, to optimize thermal performance while maintaining acceptable pressure drops. By addressing both thermal and hydraulic challenges, this work provides a robust framework for designing next-generation microchannel heat sinks.

II. COMPUTATIONAL MODEL

2.1 Design Parameters

The computational domain involves a rectangular microchannel, modeled based on the geometric specifications from Qu and Mudawar's (2002) [8] study. The microchannel features a series of parallel rectangular channels, each 231 μm wide and 713 μm deep, fabricated into a high thermal conductivity substrate such as copper. This configuration provides a high surface area for heat transfer while minimizing flow resistance. This microchannel has been shown in Fig.1

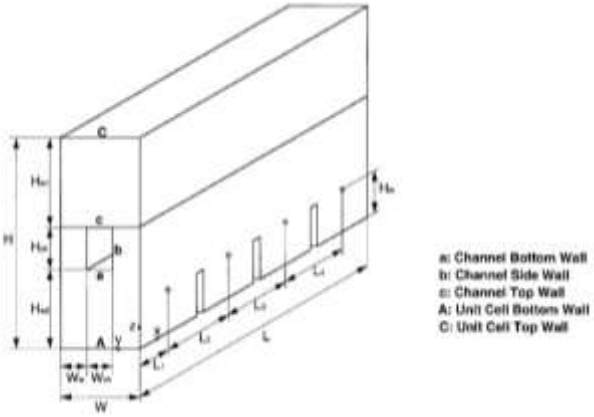

Fig 1: Schematic of heat sink unit cell for numerical simulation[8].

e-ISSN: 2582-5208
International Research Journal of Modernization in Engineering Technology and Science
(Peer-Reviewed, Open Access, Fully Refereed International Journal)
Volume:07/Issue:01/January-2025 Impact Factor- 8.187 www.irjmets.com

In this design, the flow path is optimized for maximum thermal performance by utilizing deionized water as the cooling medium. The flow regime is characterized by Reynolds numbers ranging from 400 to 1200 for heat flux levels up to 200 W/cm^2, ensuring efficient convective heat transfer. The geometry is particularly suitable for applications requiring efficient thermal management, such as electronics cooling. It balances heat transfer performance with manageable pressure drops, ensuring that the design remains practical for high-power systems. The computational analysis of this design captures both fluid and solid domains, enabling a comprehensive evaluation of conjugate heat transfer effects and thermal gradients across the microchannel walls. Based on the specified dimensions, the microchannel has been designed. The computational domain corresponding to the dimensions shown in Fig.2 has been considered.

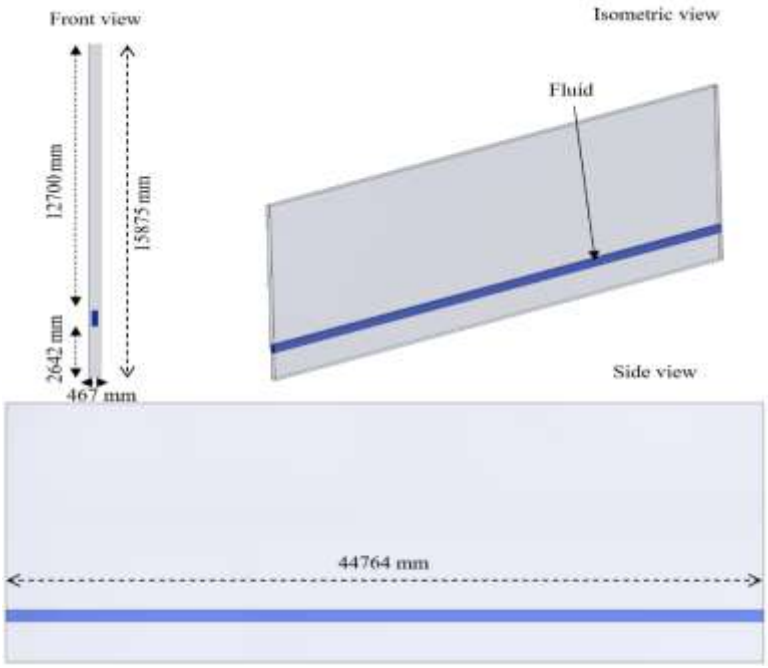

Fig 2: 3-D computational domain of single micro-channel

2.2 Governing Equations

The governing equations employed in this study are based on the fundamental principles of fluid mechanics and heat transfer. The following presumptions apply to the microchannel governing equations:

- The fluid flow and heat transfer are considered steady state.
- The fluid (water) is assumed to be incompressible.
- The flow is assumed to be laminar.
- Radiative heat transfer is neglected.
- The properties of the fluid and solid (copper metal), except for the viscosity of water, are assumed constant.
- The natural heat transfer of trapped air between the microchannel gaps is neglected.

Based on the assumptions outlined above, the governing equations for the problem are the continuity, momentum, and energy equations:

$$\nabla.\left(\rho_f\vec{V}\right) = 0 \tag{1}$$

$$\nabla.\left(\rho_f\vec{V}.\nabla\vec{V}\right) = -\nabla P + \nabla.\mu_f\left[\left(\nabla\vec{V} + \nabla\vec{V}^t\right) - {}^2/_3\,\nabla.\vec{V}\right] + \rho_f\vec{g} \tag{2}$$

$$\nabla.\left(\rho_f C_p\vec{V}T\right) = \nabla.\left(k_f\nabla T\right) \tag{3}$$

For the solid region, $\vec{V}$=0, and only the energy equation needs to be solved:

$$k_s\nabla^2 T = 0 \tag{4}$$

The inlet boundary conditions are specified as constant velocity and temperature:

e-ISSN: 2582-5208
International Research Journal of Modernization in Engineering Technology and Science
(Peer-Reviewed, Open Access, Fully Refereed International Journal)
Volume:07/Issue:01/January-2025 Impact Factor- 8.187 www.irjmets.com

$$U = U_{in} \quad (5)$$

$$T=T_{f.in} \quad (6)$$

where U_{in} = 1.15, 1.99, 2.6, 3.32, 3.98 m/s and $T_{f,in}$ =288.15K. A continuous heat flux (Equation 4) and temperature (Equation 6) are imposed as interface conditions between the solid and fluid regions:

$$-k_f \frac{\partial T}{\partial n} \text{ł}_\Gamma = -k_s \frac{\partial T}{\partial n} \text{ł}_\Gamma \quad (7)$$

$$T_{f.\Gamma} = T_{s.\Gamma} \quad (8)$$

$$\vec{V} = 0 \quad (9)$$

It is assumed that the flow at the outlet is fully developed in both hydraulic and thermal terms:

$$\frac{\partial \vartheta_x}{\partial x} = 0 \; ; \frac{\partial \vartheta_y}{\partial y} = 0 \; ; \frac{\partial \vartheta_z}{\partial z} = 0 \quad (10)$$

$$\frac{\partial^2 T}{\partial x^2} = 0 \quad (11)$$

The boundary condition at the top wall of the cell (wall C in the Fig.1) is specified as natural convection, expressed by Equation 12:

$$-k_s \frac{\partial T}{\partial z} = h_{conv}(T - T_\infty) \quad (12)$$

The performance of microchannel is often evaluated through key dimensionless and thermodynamic parameters:

Reynolds Number (*Re*): The Reynolds number quantifies the flow regime within the channel and is calculated using:

$$Re_l = \frac{\rho_f u_m D_h}{\mu_f} \quad (13)$$

where ρ_f is fluid density, u_m is mean velocity, D_h is the hydraulic diameter, and μ_f is dynamic viscosity. This number helps distinguish between laminar and turbulent flows, which directly influence thermal performance.

Nusselt Number *(Nu*): The Nusselt number represents the ratio of convective to conductive heat transfer and is given by:

$$Nu = \frac{h.D_h}{k_f} \quad (14)$$

where h is the heat transfer coefficient and k_f is the thermal conductivity of the fluid. It serves as a critical indicator of the heat transfer enhancement within the channel.

Heat Transfer Coefficient (h): The average convective heat transfer coefficient is derived using:

$$h = \frac{q.A_q}{A_c.(T_c - T_f)} \quad (15)$$

where q is the applied heat flux, A_q is the area of the heat flux application, A_c is the cooling surface area, T_c is the average conjugate area temperature, and T_f is the fluid temperature. This coefficient reflects the efficiency of heat removal.

The average fluid temperature (T_f) and the temperature at the conjugate surface (T_c) provide insights into the thermal behavior of the system. These values are integral to understanding the distribution and dissipation of heat within the microchannel.

The hydraulic diameter (D_h) is a crucial geometric parameter used to characterize the flow behavior in non-circular conduits, such as rectangular microchannels. It is defined by the equation:

$$d_h = \frac{2WH}{W + H} \quad (16)$$

e-ISSN: 2582-5208
International Research Journal of Modernization in Engineering Technology and Science
(Peer-Reviewed, Open Access, Fully Refereed International Journal)
Volume:07/Issue:01/January-2025 Impact Factor- 8.187 www.irjmets.com

where W is the channel width and H is the channel height.

2.3 Boundary Conditions and simulation setup

Since the outlet velocity is not specified, the outlet boundary condition is defined as a Pressure Outlet with zero relative static pressure and a temperature of 288.15 K. Due to the symmetry of the problem, the Symmetry boundary condition is applied to the side walls of the microchannel cell. At the top wall of the microchannel cell, air flows with forced convection, having a heat transfer coefficient of$10\frac{w}{m^2c}$ and a temperature of 298.15 K. Heat fluxes of $100\frac{W}{cm^2}$ and $200\frac{W}{cm^2}$ are applied to the bottom wall of the microchannel cell. All other outer walls of the cell are considered adiabatic. Fig.14 provides a schematic representation of the described boundary conditions.

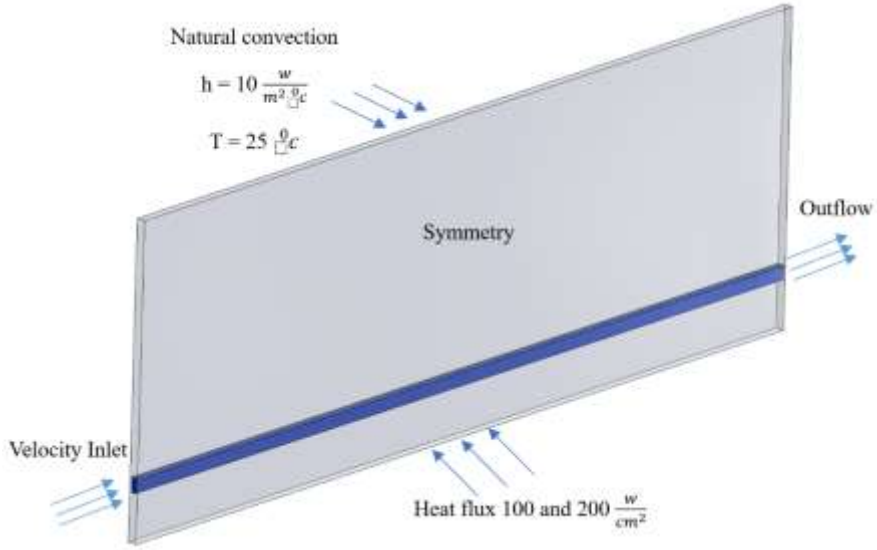

Fig 3: Boundary conditions in the rectangular microchannel

These boundary conditions ensure realistic replication of the operating environment for the microchannels.

The simulation uses water as the working fluid, with its hydrodynamic properties based on Modawar[8], and the microchannel material is copper, utilizing mechanical properties from the software's database. Four contact surfaces between the fluid and solid are designated as "Interface," with energy exchange modeled as "Coupled Wall." The SIMPLE algorithm was chosen for coupling velocity and pressure variables due to its stability, particularly in cases with skewed meshes. For discretization, the Second Order Upwind method was used for momentum and energy equations, while the Standard method was employed for pressure interpolation. Gradient calculations were performed using the Least Squares Cell-Based method, which is particularly effective for polyhedral meshes. Residual criteria for solution convergence were defined as 1×10^{-4} for velocity equations, 1×10^{-6} for the continuity equation, and 1×10^{-7} for the energy equation, ensuring accurate and stable results.

To validate the numerical accuracy, a grid independence study was performed using three different mesh element numbers: 167,073, 782,514, and 2,132,611. The results indicated that the medium mesh (782,514 elements) provided a good balance between computational cost and accuracy, with negligible differences in Nusselt number and pressure drop compared to the finer mesh. Consequently, the medium mesh was used for all subsequent simulations.

III. RESULTS AND DISCUSSION

3.1 Validation of CFD Results with Experimental Data

To validate the accuracy of the CFD simulations, the pressure drop results for simple microchannels were compared with experimental data from Qu and Mudawar[8]. The comparison was performed for two heat flux levels, $100\frac{W}{cm^2}$ and $200\frac{W}{cm^2}$, over a range of Reynolds numbers from 200 to 1500.

e-ISSN: 2582-5208
International Research Journal of Modernization in Engineering Technology and Science
(Peer-Reviewed, Open Access, Fully Refereed International Journal)
Volume:07/Issue:01/January-2025 Impact Factor- 8.187 www.irjmets.com

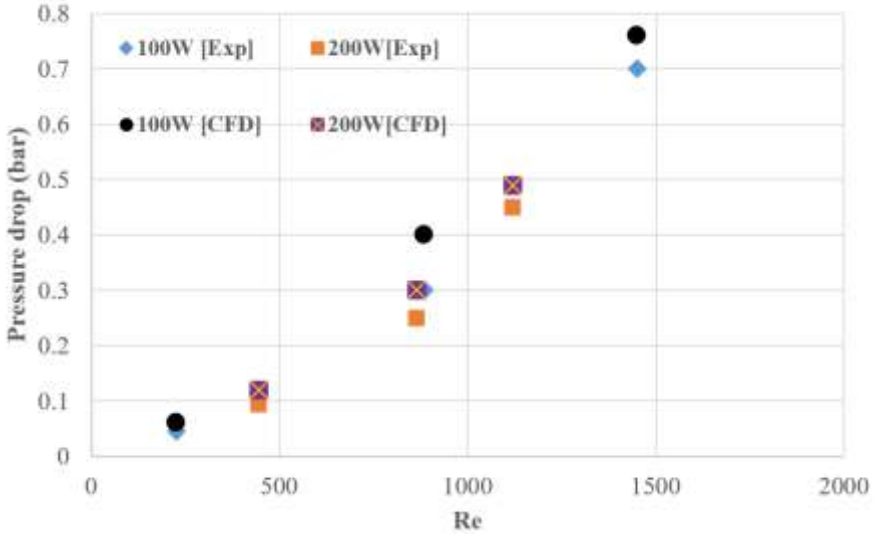

Fig 4: Pressure drops for experiment [8] and CFD.

The comparison between experimental and CFD results for 100W and 200W heat fluxes shows decreasing error percentages at higher Reynolds numbers. For 100W, the maximum error is 25% at lower Reynolds numbers, reducing to 7.89% at Re=1120. Similarly, for 200W, the error decreases from 21.67% at Re=445 to 8.16% at Re=1120. This indicates improved agreement between CFD and experimental results as Reynolds number increases. The consistent trends between CFD and experimental data indicate that the numerical model accurately captures the dominant fluid flow and thermal mechanisms.

The validation of the CFD model establishes a strong foundation for further analysis and optimization of microchannel designs, ensuring reliability in predicting performance under practical operating conditions.

3.2 Geometry optimization

3.2.1 Pin configurations

Following the validation of the CFD model with experimental data, the next phase focuses on optimizing the microchannel geometry to enhance its thermal and hydraulic performance. The study investigates the impact of pin configurations within the microchannel by exploring three distinct arrangements. Each pin has a diameter of 60 μm and a height of 400 μm. In the first configuration, a set of 5 pins is positioned at the entrance of the microchannel. The second configuration places the 5 pins at the exit, maintaining a uniform spacing between them. Lastly, the third configuration incorporates 10 pins distributed evenly along the length of the microchannel, from the entrance to the exit. These configurations aim to disrupt boundary layers, enhance turbulence, and improve heat transfer efficiency while minimizing pressure drop. Fig.5 illustrates the schematic representation of the pin configurations within the microchannel.

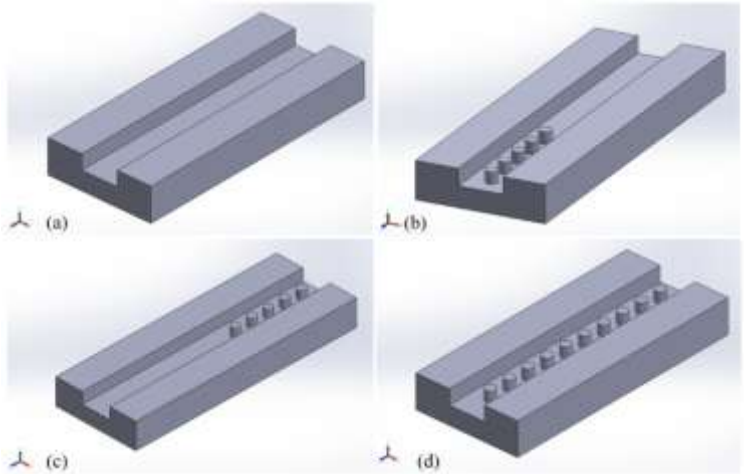

Fig 5: Pin configuration, (a)Without pin, (b) Entrance, (c) Exit, (d) Complete

e-ISSN: 2582-5208
International Research Journal of Modernization in Engineering Technology and Science
(Peer-Reviewed, Open Access, Fully Refereed International Journal)
Volume:07/Issue:01/January-2025 Impact Factor- 8.187 www.irjmets.com

The upper part of the microchannel has been removed from the schematic as it does not significantly contribute to increasing heat transfer. Additionally, this simplification reduces computational cost and allows a clearer focus on the effect of the pins. All configurations were performed for five different Reynolds numbers: 400, 600, 800, 1000, and 1200. This range was chosen to enable a thorough analysis of performance across varying flow conditions. Velocity contour for front configuration in Reynolds 400 and $100\frac{W}{cm^2}$ heat flux has been shown in Fig.6.

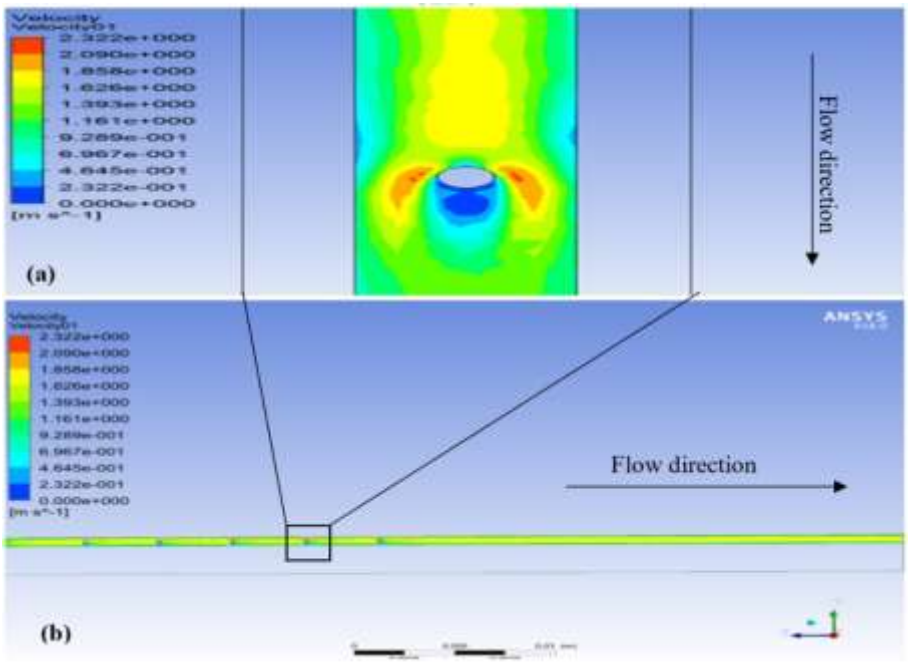

Fig 6: Velocity contour at Reynolds 400 and heat flux of 100 W/cm^2, (a) around pin number 4, (b) all pins.

The velocity contour indicates high velocity regions around the front sides of the pins due to flow acceleration caused by constriction, as shown in Fig.6 (a). Behind the pins, low-velocity zones are visible, suggesting wake formation and vortex shedding caused by flow separation. These dynamics highlight the impact of pin-induced flow disturbances, enhancing mixing but potentially increasing pressure losses. Fig.7 shows the velocity distribution for complete pin configurations.

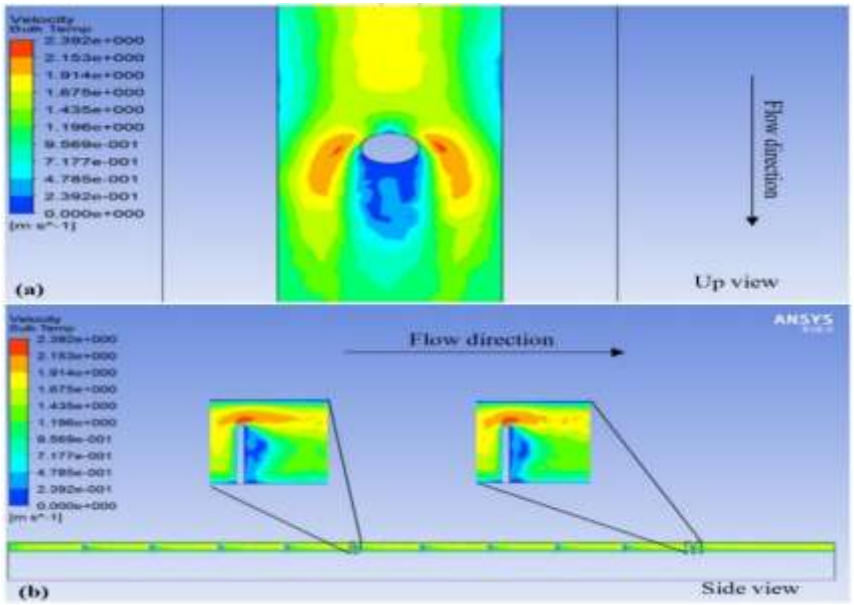

Fig 7: Velocity contour at Reynolds 400 and heat flux of 100 W/cm^2, (a) velocity contour around pin number 10, (b) velocity contour around all the pins.

e-ISSN: 2582-5208
International Research Journal of Modernization in Engineering Technology and Science
(Peer-Reviewed, Open Access, Fully Refereed International Journal)
Volume:07/Issue:01/January-2025 Impact Factor- 8.187 www.irjmets.com

The velocity contour around Pin 10 shows significant acceleration at the front of the pin, indicating high-velocity regions caused by flow constriction. Behind the pin, wake regions with low velocity are visible, highlighting flow separation and vortex formation. These patterns illustrate how the pin disrupts the flow, promoting mixing but potentially contributing to pressure losses and thermal performance enhancement.

To evaluate the convective heat transfer performance of the microchannel, the variation of the Nusselt number across all configurations has been calculated. The results, presented in Fig.8, provide valuable insights into how different configurations and Reynolds numbers influence the heat transfer efficiency within the microchannel.

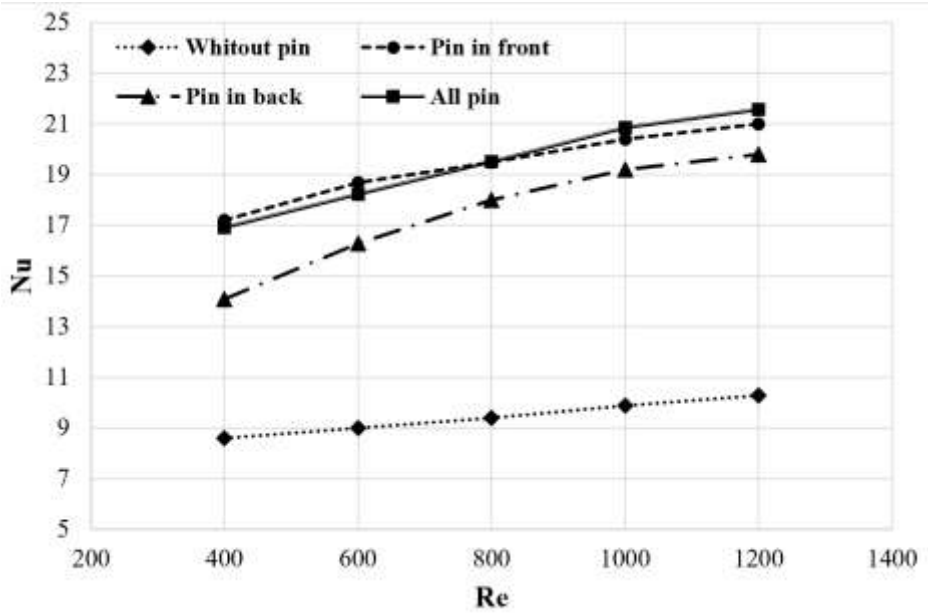

Fig 8: Comparison of the Nusselt number for four microchannel configurations at a heat flux of 100 W/cm^2

Fig.8 demonstrates that the Nusselt number (Nu) increases consistently with Reynolds number for all configurations, indicating improved convective heat transfer as flow velocity rises. The "All Pin" configuration shows the most substantial enhancement, with Nu values consistently 45–50% higher than the baseline (without pins), driven by sustained turbulence and mixing along the entire channel length. Similarly, the "Pin in Front" configuration achieves a steady improvement of 45–50%, as the early introduction of pins effectively generates turbulence and maintains its impact throughout the channel. The "Pin in Back" configuration also demonstrates consistent performance, with Nusselt number increases of approximately 35–40%, as the turbulence introduced at the channel exit effectively enhances downstream thermal mixing. These results highlight that all pin configurations deliver significant and stable heat transfer improvements compared to the baseline, regardless of Reynolds number.

It was determined that microchannels with extended thermal surfaces improve thermal performance; however, these surfaces also relatively increase the pressure drop in rectangular microchannels. To evaluate the performance of microchannels with extended surfaces compared to flat rectangular microchannels, the thermal performance parameter, as expressed by Equation 17, must be calculated.

$$\eta = \frac{Nu/Nu_0}{\left(\Delta P/\Delta P_0\right)^{1/3}} \qquad (17)$$

In this equation, the parameter Nu_0 represents the Nusselt number obtained for the without pin-fin microchannel, and the parameter ΔP_0 represents the pressure drop obtained for the microchannel without pin-fins. The graph in Fig.9 illustrates the variations of the thermal performance factor against changes in the Reynolds number.

e-ISSN: 2582-5208
International Research Journal of Modernization in Engineering Technology and Science
(Peer-Reviewed, Open Access, Fully Refereed International Journal)
Volume:07/Issue:01/January-2025 Impact Factor- 8.187 www.irjmets.com

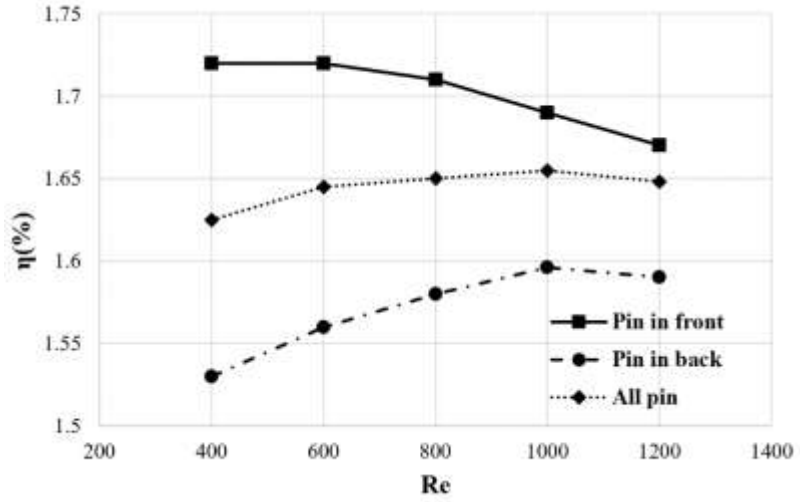

Fig 9: The thermal performance factor for three microchannels with different pin-fin arrangements at a heat flux of 100 W/cm^2

Fig. 9 shows the thermal performance factor (η) for different pin configurations across Reynolds numbers. At low Reynolds numbers, the "Pin in Front" configuration demonstrates the highest thermal performance, outperforming the "All Pin" configuration by 6% and the "Pin in Back" configuration by 12%. This significant advantage highlights the early turbulence generation provided by the "Pin in Front" configuration, which effectively balances enhanced heat transfer with manageable pressure drops. At high Reynolds numbers, the "Pin in Front" configuration continues to outperform the other configurations, though the differences become less pronounced. It exceeds the "All Pin" configuration by 2% and the "Pin in Back" configuration by 5%, maintaining its advantage as the most efficient design. These results emphasize that the "Pin in Front" configuration consistently offers the best thermal performance across all Reynolds numbers, though the relative differences between configurations decrease as the Reynolds number increases.

3.2.2 Pin height configuration

The previous section demonstrated that a flat microchannel with pin with 400 μm height arrangements at the front of the channel exhibits superior performance in reducing temperature and dissipating heat flux compared to the other configurations. Consequently, the analysis of pin height effects on the thermal performance of the microchannel focuses exclusively on the rectangular microchannel with pins positioned at the front. Two pin heights, 500 μm and 600 μm, will be examined. Fig.10 illustrates the velocity contour values for a rectangular microchannel with a pin height of 600 μm.

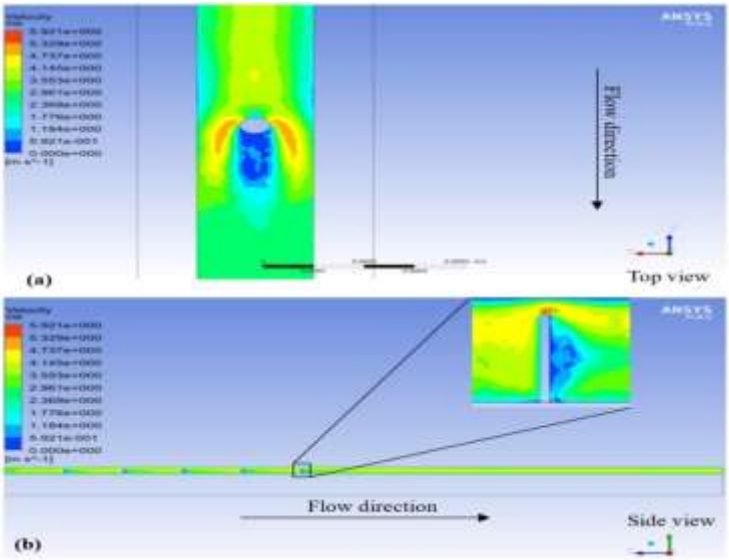

Fig 10: The velocity contour for Reynolds number of 1000 and heat flux of 100 W/cm^2.

e-ISSN: 2582-5208
International Research Journal of Modernization in Engineering Technology and Science
(Peer-Reviewed, Open Access, Fully Refereed International Journal)
Volume:07/Issue:01/January-2025 Impact Factor- 8.187 www.irjmets.com

In section (a), the velocity at the channel inlet is 2.87 m/s, increasing to 4.7 m/s near the channel exit, with the maximum velocity above the pin where the pressure is lowest. Blue regions behind the pin indicate vortex zones with low velocity, while velocity increases downstream. In section (b), the top view of the fifth pin shows similar vortex zones (blue) with lower velocities, while high-velocity areas (red) occur where the pressure gradient is negative ($dp/dz<0$). The separation point, marked by $dp/dz=0$, occurs at the rear of the cylinder where the flow lacks momentum to overcome the adverse pressure gradient. This causes boundary layer separation, forming a wake region with irregular, vortex-filled flow downstream.

The graph in Fig.11 illustrates the variations in the Nusselt number as a function of the Reynolds number for a pin height of 600 µm.

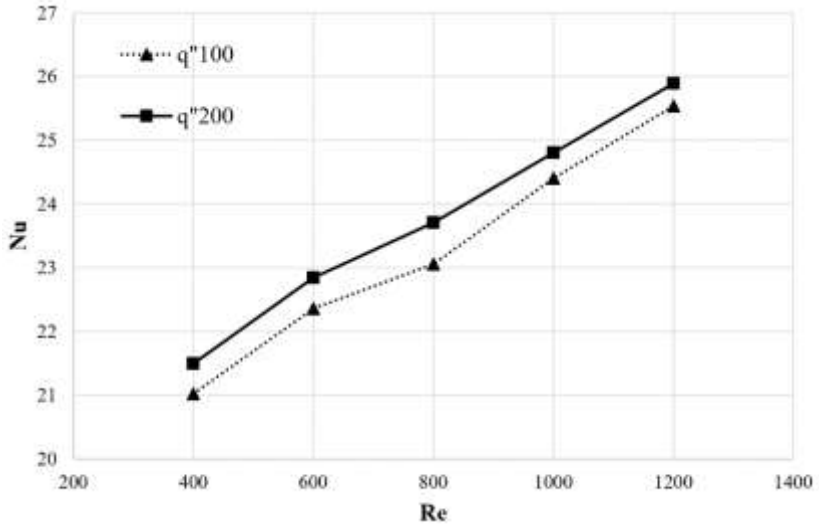

Fig 11: Variations in the Nusselt number respect to the Reynolds number for a pin height of 600 µm.

The chart illustrates the variation of the Nusselt number (Nu) with Reynolds number (Re) for two different heat flux conditions: q'' = 100W/cm² and q'' = 200W/cm². For both heat fluxes, Nu increases consistently with Re, indicating enhanced convective heat transfer performance at higher flow rates. The q'' = 200W/cm² configuration consistently exhibits slightly higher Nu values than q'' = 100W/cm², reflecting the impact of greater heat flux on thermal efficiency. This trend highlights the dependence of heat transfer performance on both flow conditions and applied heat flux.

To facilitate a comparison of the four specified pin heights, the results are illustrated in a graphical format. Fig.12 presents the relationship between the Nusselt number and pin height for Reynolds numbers of 400 and 1000, providing a clear depiction of the performance variations across different configurations.

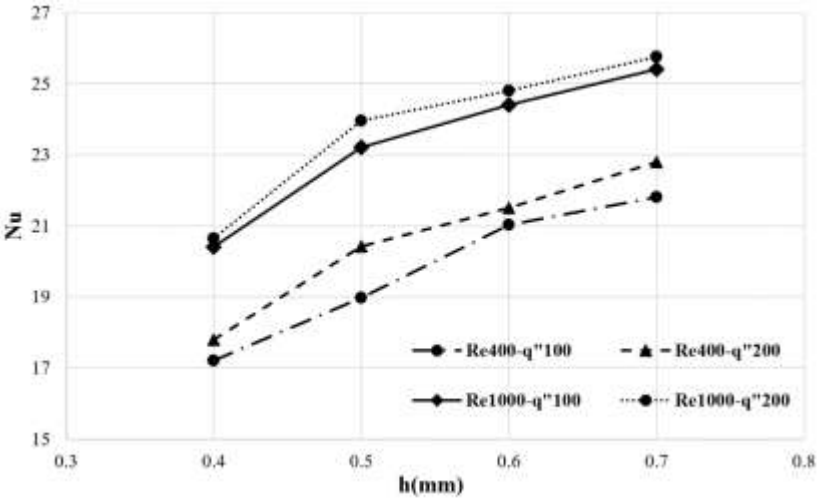

Fig 12: Changing Nusselt number for different pin heights.

Fig.12 illustrates the relationship between the Nusselt number (Nu) and pin height, ranging from 400 μm to 700 μm, across Reynolds numbers of 400 and 1000. The data clearly shows that increasing pin height enhances the Nusselt number due to the greater heat transfer surface area and intensified turbulence. At low Reynolds numbers (Re = 400) with a heat flux of 100 W/cm^2, increasing the pin height from 400 μm to 700 μm leads to a significant Nusselt number improvement of 22.5%, demonstrating the substantial impact of taller pins in low-flow conditions. At high Reynolds numbers (Re = 1000), the same increase in pin height results in a Nusselt number improvement of 20.5%, slightly lower than at low Reynolds numbers but still substantial. This difference indicates that while taller pins remain effective at higher Reynolds numbers, the relative benefit decreases slightly as flow velocity increases due to reduced sensitivity to surface modifications. Overall, the results highlight that optimizing pin height is critical for maximizing heat transfer efficiency, with the most significant improvements observed at lower Reynolds numbers.

IV. CONCLUSION

This research demonstrates the significant impact of geometric modifications, particularly pin configurations, and heights, on the thermal and hydraulic performance of rectangular microchannels. Among the evaluated configurations, the "Pin in Front" design consistently provides the highest thermal performance, outperforming the "All Pin" configuration by 6% and the "Pin in Back" configuration by 12% at low Reynolds numbers. At higher Reynolds numbers, the "Pin in Front" configuration retains its advantage, with 2% and 5% improvements over the "All Pin" and "Pin in Back" configurations, respectively. Additionally, increasing the pin height from 400 μm to 700 μm results in a Nusselt number improvement of 22.5% at low Reynolds numbers and 20.5% at high Reynolds numbers, demonstrating the critical role of pin dimensions in enhancing heat transfer. These results underscore the necessity of optimizing microchannel designs to achieve a balance between enhanced thermal performance and acceptable pressure drops. Future research could explore additional parameters such as varying pin shapes, spacing, and material properties to further advance the thermal management capabilities of microchannels in high-power electronic systems.

V. REFERENCE

[1] Yuan, X.; Tao, Z.; Li, H.; Tian, Y. Experimental Investigation of Surface Roughness Effects on Flow Behavior and Heat Transfer Characteristics for Circular Microchannels. Chinese Journal of Aeronautics 2016, 29, 1575–1581, doi:10.1016/j.cja.2016.10.006.

[2] Datta, A.; Sanyal, D.; Das, A.K. Numerical Investigation of Heat Transfer in Microchannel Using Inclined Longitudinal Vortex Generator. Appl Therm Eng 2016, 108, 1008–1019, doi:10.1016/j.applthermaleng.2016.07.165.

[3] Xia, G.; Ma, D.; Zhai, Y.; Li, Y.; Liu, R.; Du, M. Experimental and Numerical Study of Fluid Flow and Heat Transfer Characteristics in Microchannel Heat Sink with Complex Structure. Energy Convers Manag 2015, 105, 848–857, doi:10.1016/j.enconman.2015.08.042.

[4] Tuckerman, D.B.; Pease, R.F.W. High-Performance Heat Sinking for VLSI. IEEE Electron Device Letters 1981, 2, 126–129, doi:10.1109/EDL.1981.25367.

[5] Sahar, A.M.; Wissink, J.; Mahmoud, M.M.; Karayiannis, T.G.; Ashrul Ishak, M.S. Effect of Hydraulic Diameter and Aspect Ratio on Single Phase Flow and Heat Transfer in a Rectangular Microchannel. Appl Therm Eng 2017, 115, 793–814, doi:10.1016/j.applthermaleng.2017.01.018.

[6] Baraty Beni, S.; Bahrami, A.; Salimpour, M.R. Design of Novel Geometries for Microchannel Heat Sinks Used for Cooling Diode Lasers. Int J Heat Mass Transf 2017, 112, 689–698, doi:10.1016/j.ijheatmasstransfer.2017.03.043.

[7] Rimbault, B.; Nguyen, C.T.; Galanis, N. Experimental Investigation of CuO–Water Nanofluid Flow and Heat Transfer inside a Microchannel Heat Sink. International Journal of Thermal Sciences 2014, 84, 275–292, doi:10.1016/j.ijthermalsci.2014.05.025.

[8] Qu, W.; Mudawar, I. Analysis of Three-Dimensional Heat Transfer in Micro-Channel Heat Sinks. Int J Heat Mass Transf 2002, 45, 3973–3985, doi:10.1016/S0017-9310(02)00101-1.

[9] Nekoubin, N. A Single Domain Formulation on Conjugate Heat Transfer in Parallel Plate Microchannel with Electrical Double Layer. International Journal of Thermal Sciences 2016, 110, 206–221, doi:10.1016/j.ijthermalsci.2016.07.003.

[10] Wang, Y.; Liu, J.; Yang, K.; Liu, J.; Wu, X. Performance and Parameter Optimization Design of Microchannel Heat Sink with Different Cavity and Rib Combinations. Case Studies in Thermal Engineering 2024, 53, 103843, doi:10.1016/j.csite.2023.103843.

[11] Ghani, I.A.; Sidik, N.A.C.; Mamat, R.; Najafi, G.; Ken, T.L.; Asako, Y.; Japar, W.M.A.A. Heat Transfer Enhancement in Microchannel Heat Sink Using Hybrid Technique of Ribs and Secondary Channels. Int J Heat Mass Transf 2017, 114, 640–655, doi:10.1016/j.ijheatmasstransfer.2017.06.103.

[12] Singh, P.K.; Harikrishna, P.V.; Sundararajan, T.; Das, S.K. Experimental and Numerical Investigation into the Hydrodynamics of Nanofluids in Microchannels. Exp Therm Fluid Sci 2012, 42, 174–186, doi:10.1016/j.expthermflusci.2012.05.004.

[13] Wei, X.; Joshi, Y.; Patterson, M.K. Experimental and Numerical Study of a Stacked Microchannel Heat Sink for Liquid Cooling of Microelectronic Devices. J Heat Transfer 2007, 129, 1432–1444, doi:10.1115/1.2754781.

[14] Kuppusamy, N.R.; Mohammed, H.A.; Lim, C.W. Numerical Investigation of Trapezoidal Grooved Microchannel Heat Sink Using Nanofluids. Thermochim Acta 2013, 573, 39–56, doi:10.1016/j.tca.2013.09.011.

[15] Li, J.; Kleinstreuer, C. Thermal Performance of Nanofluid Flow in Microchannels. Int J Heat Fluid Flow 2008, 29, 1221–1232, doi:10.1016/j.ijheatfluidflow.2008.01.005.

[16] Fallahzadeh, R.; Garousi, M.H.; Pagliarini, L.; Bozzoli, F.; Cattani, L. Single-Loop Triple-Diameter Pulsating Heat Pipes at Reduced Heat Input: A CFD Study on Inner Diameter Optimization. Energies (Basel) 2024, 17, 5568, doi:10.3390/en17225568.

[17] Garousi, M.H.; Karimi, M.; Casoli, P.; Rundo, M.; Fallahzadeh, R. Vibration Analysis of a Centrifugal Pump with Healthy and Defective Impellers and Fault Detection Using Multi-Layer Perceptron. Eng 2024, 5, 2511–2530, doi:10.3390/eng5040131.

[18] Casoli, P.; Vescovini, C.M.; Masoud, H.G.; Rundo, M. A Novel 1D Approach for Modelling Gas Bladder Suppressors on the Delivery Line of Positive Displacement Pumps. Energies (Basel) 2024, 17, 1610, doi:10.3390/en17071610.